VNIVERSITAT DE VALÈNCIA Facultat de Física GRADO EN FÍSICA

# Trabajo de Grado

## Superluminal motion in relativistic jets

SEPTIEMBRE de 2012

Alumno/a: Enrique Sanchis Melchor

Tutor : Eduardo Ros Ibarra

# Superluminal motion in relativistic jets

**Enrique Sanchis Melchor**

Facultad de Física, Universitat de València, Spain
E-mail: ensanmel@alumni.uv.es

**Abstract**
Superluminal motions are observed in astronomy when the apparent sky velocities of certain features move at velocities faster than light. Superluminal motions are usually observed in active galactic nuclei (AGN). This apparent violation of special relativity can be explained with simple formulae as a consequence of a change in the reference frame between the related galaxy and the observer.
So far there have been identified hundreds of AGN galaxies with observed jet features classified as superluminal objects; nowadays different research groups study the kinematics of those components with the aim of acquiring a better understanding of the physics related to AGN galaxies.
We explain in this work the basics of this physical event, and go into detail with the kinematic formulation and the kinematic parameters of the observed jet regions. To finish, we will summarize recent deductions and discoveries from observations ongoing surveys of this field.

## 1. Introduction

The term superluminal motion is used when the apparent transverse velocity of an object or region of radiation is greater than speed of light. This effect can be obtained mainly in two different situations: light echoes around supernovae, and in AGN or microquasars (μQSO) with relativistic jets. The first phenomenon does not imply a motion of any object, but it occurs when different parts of an object emit light in such a sequence that radiation seems to move with $\beta_{app} > c$ (Laing *et al*. 1997 [1]), where $\beta = v/c$, $v$ is the speed of a body and $c$ the speed of light.

The second kind of superluminal event takes place at black-hole powered objects (such as μQSO or AGN), which consist of a core and of distinguishable enhanced emission regions or "features" (commonly named as components in the literature, or blobs of plasma also) which we can measure their positions relative to the center of the galaxy, after densely time sampled monitoring. If we know the distance to the host galaxy (from the redshift in AGN or from parallax measurement in galactic bodies) we can determine the apparent velocities observing the positions of each feature at different times, resulting in many of the cases to be higher than the speed of light $c$. To date, apparent speeds observed in active galactic nuclei range from subluminal speeds ($\beta_{app} < c$) to a maximum of $50c$, although common values are around 1-$10c$ (Lister *et al*. 2009 [2]). Typically, for observing changes in the AGN structure, time intervals of few months are needed.

The brief description of the event is that the jet component moving towards the observer with $\beta \to c$ is radiating light travelling at speed $c$. If we measure the time interval between two different epochs, it results lower than for the static case since the object has approached the observer between the two time epochs. As a consequence, the observed speed becomes higher than its intrinsic speed without any upper limit.

Superluminal motions were predicted by Martin Rees in 1966 and discovered in 1969, when technology made Very-Long-Baseline Interferometry (VLBI) possible. This technique studies very compact bodies in radio frequencies, among them AGN. In active galactic nuclei the radio emission is believed to be produced by synchrotron process, which happens when electrons inside a magnetic field move in spiral trajectories with relativistic speed.

This work is focused on the second type of motions faster than speed-of-light, that is to say, superluminal motion in extragalactic radio sources. This phenomenon, and AGN in general, has been extensively studied in the last decades. For an introductory text to the topic, see *e.g.*, Burke & Graham-Smith [3], J.D. Kraus [4] or others.

The text is organized as follows. *Section 1* gives an overview of the event, including basic notions about AGN and a short historical introduction. *Section 2* provides an explanation of the event from a geometrical point of view. *Section 3* develops all the associated formulae that allow a complete study of the event. *Section 4* discusses relationships between parameters involved in the mathematical description. *Section 5* summarizes recent discoveries and observed tendencies of relativistic jets, and the conclusions appear in *Section 6*.

### 1.1. AGN and quasars

Before going into detail, we should briefly talk about the kind of sources where this event is most commonly observed, mainly the AGN.

An active galactic nucleus (commonly referred as AGN) is a compact source which has a relatively much higher luminosity than a normal galaxy within a concrete range of the spectrum, or even overall. The unification model (*e.g.*, Blandford & Königl 1979 [5]) is nowadays the most accepted view of AGN. It considers that at the center of the galaxy there is a supermassive black hole, surrounded by an accretion disk. The high luminosity is originated at the central region of the system, where the black hole accretes matter from the disk.

Apart from the incoming matter from the disk, the black hole ejects matter at very high speeds forming two opposite, powerful jets. Although the mechanism of jet launching is still not fully understood, it has been suggested that the jets are caused by strongly collimated magnetic fields which are created by charged particles falling onto the black hole by dynamo processes. The power of the black hole makes that outgoing matter travels with a highly relativistic speed.

The accretion disk is made up of spinning cold matter that heats up while approaching the black hole. The electromagnetic spectrum of the disk is expected to be centered at the optical or ultraviolet wavelength, but commonly its emission spectrum is partly absorbed by dust or gas outside the accretion disk. On the other hand, the relativistic jets emit radiation of all wavebands, including radio frequencies, which can be studied via Very-Long-Baseline Interferometry. The physics and the processes that

form the jets are still not clarified, and so far VLBI observations are the best way of studying the powerful AGN jets.

The basic classification of AGN differentiates between radio-loud and radio-quiet galaxies. At radio-loud galaxies, the luminosity is mainly dominated by the jets and the lobes of the AGN, while for radio-quiet sources the emission of the jets is low and can be simplified to be only due to the central core. The observational aspect of an AGN is a function of the angle between the jet's direction and the line of sight. This angle highly modifies the observed morphology of the AGN, the optical picture is certainly different if the angle goes close to zero, or if it tends to 90º: for ~0º is considered a blazar; for an angle laying between ]0º, 90º[ would be named as quasar or Seyfert 1 Galaxy, and for ~90º would be seen as a Seyfert 2 Galaxy or a Radio galaxy. The orientation explains observed characteristics in AGN such as: high polarization, rapid variation in observations, high luminosity and –frequently- apparent speed of the jets higher than $c$. An important blazar subtype, known as BL Lacertae (or simply BL Lac) Objects, is also a common superluminal source. BL Lacs Objects (usually core-dominated radio sources) are observed to have lower luminosity than other active galactic nuclei.

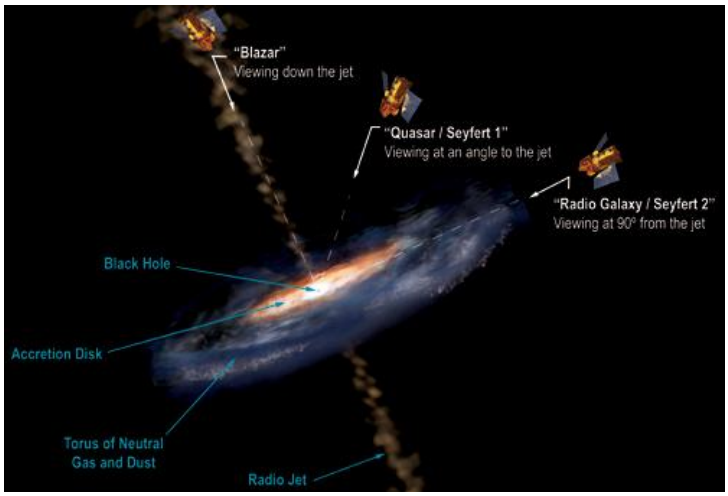


**Figure 1: observed types of AGN depending on the angle of view.** ***Image from www.nasa.gov (Aurore Simonnet, Sonoma State University)*** **[6].**

The conditions for superluminal motion require: high velocities at the rest frame near to the speed of light ($\beta \to c$) and small angles between the line of sight and the jet. To estimate the apparent linear speeds from the proper motions measured as arc distances in the sky, we need to know the distance to the objects, obtained independently.

Under these conditions blazars and quasars at small angles are typically the kind of AGN where superluminal motions are most commonly observed.

### 1.2. Historical introduction

Before the observation of the phenomenon, in 1966 *Martin Rees* predicted superluminal motion for sources coming towards an observer with relativistic transverse velocity (Rees *et al*. 1966 [7]). This is one example of a theoretical prediction coming

forward its observation, a fact that happens to be essential in nowadays physics, and particularly in astronomy.

Initially, Rees prediction was done in order to explain the recent discovery of rapid variations in the radio flux of quasars (*e.g.*, Dent 1965 [8]). Those variations presented considerable problems with the theory of radio galaxies of that epoch, which was based on the hypothesis that their emission was synchrotron radiation from expanding clouds of electrons moving with relativistic speeds inside weak magnetic fields. Rees prediction of superluminal motion was able to solve the problem without modifying the theory of radio galaxies.

The confirmation of Rees prediction had to wait until the development of a brand new technique at that time, VLBI. This technique employs several telescopes linked together and distributed along a surface, spanning us much as possible for better precision. VLBI observations made possible a resolution of miliarcseconds. During the late 1960s different groups in the U.S., Canada, England and the U.S.S.R. developed the technique and the first experimental results were obtained.

The first detection of a source moving with apparent velocity higher than speed of light was the quasar 3C 279 by an American-Australian group in 1969-1971 (Gubbay *et al*. 1969 [9]). They observed changes in the structure of the quasar that implied an apparent velocity around $2c$ for one component of the source, and they concluded (Moffet *et al*. 1972 [10]) that this speed was due to a relativistic expansion as Rees predicted in 1966.

These results attracted the attention of several physicists and researchers, and it became a controversy because some concluded those results was in fact a refutation of Special Relativity. But the improvement in the next years of the analysis methods for VLBI and resolutions gave better observations and true images were managed. More superluminal sources were determined, apparently confirming the Rees's prediction, and finally it became the most accepted explanation of these phenomena.

Around 1983 the number of well-known superluminal sources increased to just 7, but since then, and especially since the beginning of the 1990's decade due to the construction of the Very Long Baseline Array (VLBA) in the U.S and other arrays of telescopes, the number of detections rose intensively. Also in Europe the research of superluminal motion was developed since then, thanks to surveys such as the European VLBI Network (EVN), and the Long Baseline Array (with the collaboration of Australia).

Another important discovery in 1994 was the observation of a superluminal source in our own galaxy (Mirabel & Rodríguez *et al*. 1994 [11]). They found a source in our galaxy with components expanding within weeks by 0,5 arcsec, implying an apparent speed faster than light. Because the similarities to the typical superluminal sources, this phenomenon was called as *microquasar*.

## 2. Explanation of the phenomenon

Even though there are several possible explanations for this event (as the 'Christmas tree' model, the 'lighthouse' model, or more exotic models which reject special relativity; see Marscher *et al*. 1998 [12]), the most widely accepted picture is easily explained with simple geometry and basic notions of special relativity.

Roughly speaking, superluminal motion occurs when a concrete source of radiation evolves with high speed and its direction is nearly pointing toward the observer, namely, the angle between the line of sight and the velocity vector is small.

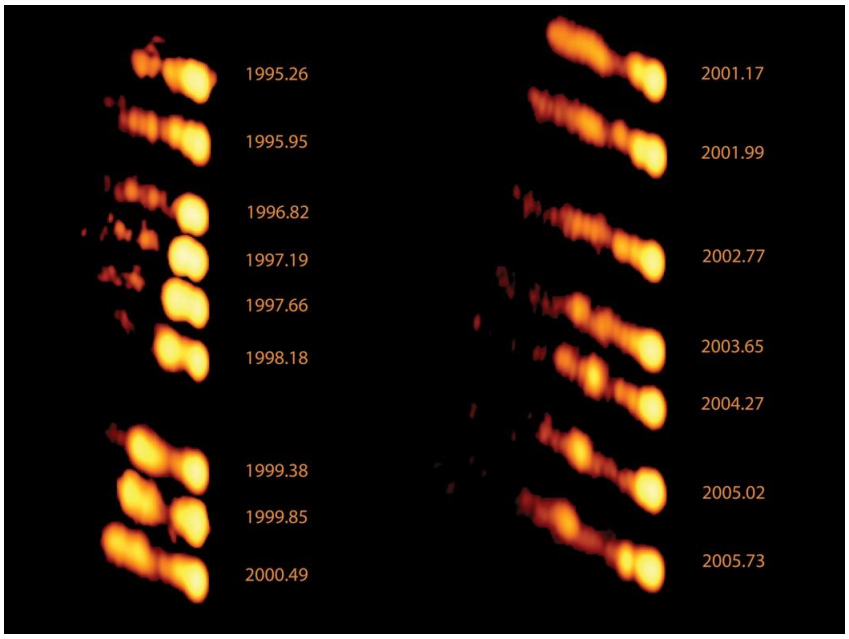


**Figure 2. Evolution of the jet of 3C 111 from 1995 to 2005 as observed with the Very Long Baseline Array. The core is located at the right side of the pictures, and the feature is ejected from the core and goes away to the left as time passes. The apparent speed ranges between 3c-6c.** ***Image courtesy of NRAO/AUI and C. Fromm, Max-Planck-Institut für Radioastronomie, Bonn, Germany*** **[13].**

First of all, we introduce the well known parameters of special relativity $\beta$ and Γ. The dimensionless $\beta$ refers to the speed of an object in natural units; while Γ is the Lorentz factor (usually the uppercase gamma is used when discussing superluminal motion, and the lowercase gamma $\gamma$ in any other field):

$$\beta = \frac{v}{c}, \qquad \text{(Eq.1)}$$

$$\Gamma = \frac{1}{\sqrt{1-\beta^2}}. \qquad \text{(Eq.2)}$$

The core (or base of the jet) is assumed to be stationary and therefore its radiation will take always the same time to reach the observer (see figure 3). In this formulation, the galaxy recession (caused by the universe's expansion) measured as a redshift $z$ is negligible; not the times measured there, which have to be corrected by a factor $(1+z)$. On the other hand, the component of the jet also emits light continuously. At an initial time the radiation is sent out from the core and from the component; we have the feature travelling almost directly toward the observer with speed near c, and its related light directed straightly to the observer with speed $c$. In a later time $\Delta t$, both have approached the observer a large quantity: the component a distance $\beta c \cdot \Delta t \cdot \cos\theta$, and $c \cdot \Delta t$ for the radiated light. The component seems to be "chasing" its radiation, and the consequence is that when the observer detects the second signal of the component, the time employed

decreases an amount $\beta \cdot \Delta t \cdot \cos\theta$, meanwhile the core's radiation takes always the same time to arrive to the observer.

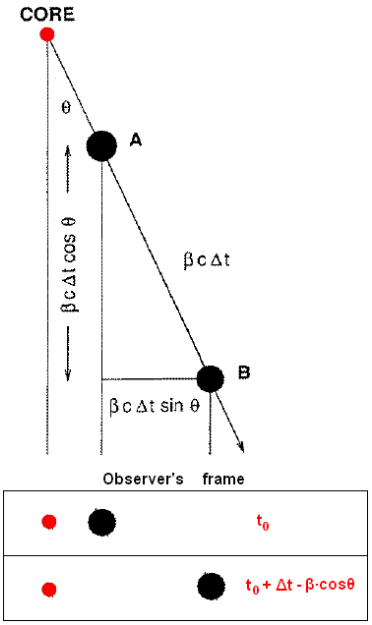


**Figure 3. Cartoon illustrating the superluminal motion phenomenon.** ***From R.A. Laing*** **[14].**

The apparent speed in the plane of the sky is the sideways distance traveled by the feature, $\beta c \cdot \sin\theta$, divided by the elapsed time between the two measurements:

$$v_{\perp app} = \frac{\beta c \cdot \Delta t \cdot \sin\theta}{\Delta t - \beta \cdot \Delta t \cdot \cos\theta} = \frac{\beta c \cdot \sin\theta}{\Delta t - \beta \cdot \cos\theta} . \qquad \text{(Eq.3)}$$

The resulting formula indicates that the measured apparent velocity of the jet's component is increased for relativistic features and can be higher than speed of light for small values of angle $\theta$. Superluminal motion occurs if $v_{\perp app} > c$, and from equation 3 this will take place when $\beta \cdot (\sin\theta + \cos\theta) > 1$.

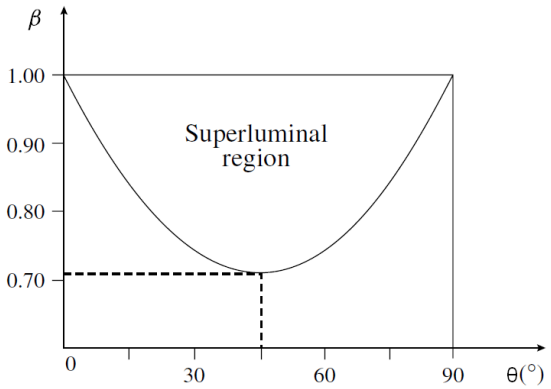


**Figure 4. Superluminal region for a linearly expanding source, shown as an area on the $\beta - \theta$ diagram.** ***From D.F. Falla & M.J. Floyd*** **[15].**

The maximum value of apparent transverse velocity is $v_{crit} = \beta c \cdot \Gamma$, and is reached when $\cos\theta \equiv \beta$.

Actually, VLBI observations measure the apparent transverse angular speed of the feature $\mu_{\perp app}$, so for obtaining the apparent velocity we should multiply that angular speed by the distance $d$ to the source, and consider also the time dilation caused by the galactic recesion expressed as a function of the redshift $z$:

$$v_{\perp app} = (1+z) \cdot d \cdot \mu_{\perp app} \, . \qquad \text{(Eq.4)}$$

Relativistic Doppler boosting (treated at *section 3.1*) prevents most receding jets from being observed, but in few cases, the two opposing jets of the active galaxy have been observed (see *Section 5*). When this happens, the distance to the source and the rest frame velocity can be determined without any other kind of observations.

The importance of superluminal motions in astronomy lies in the use of the kinematical properties of jets for determining its physical nature and, in general, for improving our understanding of AGN. Although current theory of radio galaxies assumes that the acceleration of the jets is related with strong magnetic fields due to the central black hole and the accretion disk (*e.g.*, Meier *et al*. 2001 [16]), there are still many unsolved points about the physics of these galaxies and all the associated formulae. The relation between the engine within the core and the components of the jets is still not well understood, and neither its connection to the jet kinematics. Other questions could be: if $\gamma$-rays come from relativistic shocks; which mechanisms take place in the emission and in the energy dissipation from the core; relation between radio spectrum and $\gamma$-rays. The details on these studies are beyond the scope of this work.

## 3. Development of the formulae

In this part of the work we develop all the mathematical relations to apply them to the experimental data from observations.

### 3.1.Doppler beaming

So far we described the effect of relativistic speeds from the point of view of its geometry; that causes the illusion of an apparent velocity higher than $c$. But for the observer, another important characteristic of the phenomenon is the Doppler factor (represented with $\delta$), which modifies the apparent luminosity of the source. This effect, also known in literature as *Doppler boosting* or *relativistic beaming*, enhances the radiation of the source that is moving toward the observer, and decreases the radiation with opposite direction.

The Doppler beaming is an effect of the well known Doppler effect, but applied to electromagnetic waves, which in the studied event is light from astronomical sources. The wave advancing towards the observer is seen to have a shorter wavelength, and therefore a higher apparent frequency. Energy is directly proportional to this frequency ($E = \hbar \cdot \nu$), and luminosity is simply energy per unit time. Apparent luminosity is

enhanced by the Doppler factor as follows (with parameter $n$ depending on the jet geometry, this factor can be 2 or 3):

$$L_{app} = L_{intrinsic} \cdot \delta^n \ . \qquad \text{(Eq.5)}$$

As a consequence, in blazars the jet pointed to us would be observed with an apparent luminosity higher than at its rest frame, while the opposite jet would appear dimmer to the point of undetectability. This is the reason why almost all the quasars are observed to have a one-sided jet structure, with a unique jet pointing towards the observer: the counterjet is not observed because its low apparent luminosity. But there are some examples showing both jet and counterjet, like NGC 1052 (Vermeulen *et al.*, 2004 [17]), 3C 84 (Walker et al., 1994 [18]): those are always detectable radio galaxies or compact symmetric objects at much closer distances to us (so with lower intrinsic luminosities).

The Doppler boosting depends on the geometry of the event, concretely on the Lorentz factor Γ, and on $\theta$ (angle between line of sight and the jet direction):

$$\delta = \Gamma^{-1} \cdot (1 - \beta \cdot \cos\theta)^{-1}. \qquad \text{(Eq.6)}$$

When the Doppler factor is not negligible, it modifies several measurable quantities on the observations. Compared to a stationary source, the increment of brightness is boosted by a factor of $\delta^n$ as we discussed before. From equation 6, Doppler bosting can also affect the values of $\theta$ and Γ.

Doppler beaming help astronomers to the comprehension of AGN, in such a way that it could help to explain their broad-band energy emission (*e.g.*, Lister *et al.*, 2011 [19]). The overall spectrum of AGN is composed of both emissions from the core and from the jets. Therefore knowing the boost of the jet's radiation we could identify the part of the spectrum due to the core and the remaining part due to the material flow of the jets.

### 3.2. Non-accelerating object

Let us consider an object emitting signals and moving towards the observer with a certain velocity. If the speed is high enough, there are two different effects we have to consider: relativistic transformations and the signal delay due to the time travel of light. The relativistic transformation is related to changes on the reference frame (galaxy's frame and observer's frame), but for most of the observed superluminal sources this effect is not relevant because the two reference frames don't move with high relativistic speeds. The signal-delay transformation formula (SDT) takes into account the time needed for the light to reach the observer. At time $t_0$ the observer is placed at the origin, and a moving source at point ($x = x_0$, $y = 0$) emits a signal. The observer will measure the signal at time:

$$t_0^{obs} = t_0 + \frac{x_0}{c} \quad Signal - \text{Delay Transformation } (SDT). \qquad \text{(Eq.7)}$$

At time $t_0$ the source is at a distance $d$ from the observer and moves with an angle $\theta$ respect to the line of sight towards him. At time $t_1$ the object is now at position ($x = x_1$, $y = y_1$) and has moved a distance $r = v(t_1 - t_0)$ (see figure 5).

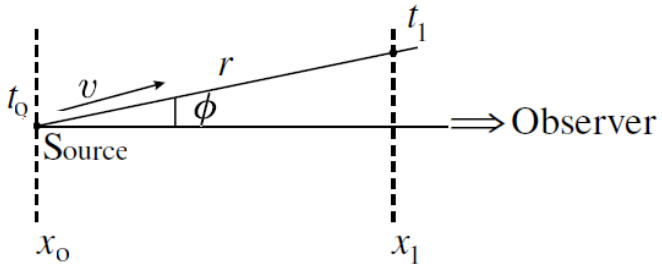


**Figure 5. A source moving linearly towards the observer with velocity $v$. *From Falla & Floyd* [15].**

We can obtain the distance $r$ relative to the time measured by the observer $t_{obs}$ using the SDT equation:

$$t_{0,1}^{obs} = t_{0,1} + \frac{x_{0,1}}{c}, \qquad \text{(Eq.8)}$$

$$x_1 - x_0 = r \cdot \cos\theta\,, \qquad \text{(Eq.9)}$$

$$t_{obs} \equiv t_1^{obs} - t_0^{obs} = (t_1 - t_0) + \left(\frac{x_1}{c} - \frac{x_0}{c}\right), \qquad \text{(Eq.10)}$$

$$t_{obs} = r\left(\frac{1}{v} - \frac{\cos\theta}{c}\right). \qquad \text{(Eq.11)}$$

In real observations we get the apparent transverse velocity $v_{\perp app}$ from the apparent angular motion $\mu_\perp$ (the distance $D$ to the source relates these two parameters as $v_{\perp app} = D \cdot \mu_\perp$). From figure 5 it is easy to find that $v_{\perp app} = r \cdot \sin\theta / t_{obs}$. Therefore we finally get:

$$v_{\perp app} = \left(\frac{1}{v} - \frac{\cos\theta}{c}\right)^{-1} \cdot \sin\theta, \qquad \text{(Eq.12)}$$

$$v_{\perp app} = \frac{\beta \cdot c \cdot \sin\theta}{1 - \beta \cdot \cos\theta}, \qquad \text{(Eq.13)}$$

$$\beta_{\perp app} = \frac{\beta \cdot \sin\theta}{1 - \beta \cdot \cos\theta}. \qquad \text{(Eq.14)}$$

There exists a maximum value of the apparent velocity known as critical velocity $\beta_{crit}$. If we derive the above equation and equal it to zero, we get straightforward this value:

$$\beta_{crit} = \sqrt{\Gamma^2 - 1}\,. \qquad \text{(Eq.15)}$$

And it happens when angle $\theta \equiv \cos^{-1}\beta = \theta_{crit}$. From this we can deduce a minimum value of the velocity $\beta$ that could yield superluminal motion. This occurs at angle $\theta = 45°$ and gives a lower value of $\beta > 2^{-1/2}$. In other words, for velocities lower than $2^{-1/2}$ superluminal motion is not possible at all.

Changes in angle $\theta$ during motion will affect to the value of the apparent velocity of the feature (and to the parallel acceleration as we will see in *section 3.3*). Therefore, if we observe a variation in the apparent velocity (assuming the intrinsic velocity approximately constant) we could suppose that the variation is due to a change in the angle $\theta$. In *section 3.4* we will see that a change in $\theta$ would also imply a variation in the observed luminosity of the feature, and this can help us to diagnose the change in $\theta$.

### 3.3. Accelerating object

The source can turn in any way and accelerate, so in general $\dot{\beta} \neq 0$. From now we will be more accurate about reference frames and we will consider the possibility of relativistic transformations. For doing that we define three different time frames (Homan *et al*. 2009 [20]):

- Time $t$ is the time associated to the rest frame (the host galaxy frame).
- $t_{obs}$ includes the signal delay of the motion.
- $t'_{obs}$ is the real time measured at the observer's frame, does include relativistic transformations due to the redshift.

With this convention, we can define the derivatives of the velocity, the Lorentz factor, the apparent velocity and the apparent angular motion:

$$\dot{\beta} = \frac{d\beta}{dt}\,, \qquad \text{(Eq.16)}$$

$$\dot{\Gamma} = \frac{d\gamma}{dt} = \dot{\beta}\cdot\beta\cdot\gamma^3\,, \qquad \text{(Eq.17)}$$

$$\dot{\beta}_{app} = \frac{d\beta_{app}}{dt_{obs}}\,, \qquad \text{(Eq.18)}$$

$$\dot{\mu} = \frac{d\mu}{dt'_{obs}} = \frac{d\mu}{dt_{obs}}\cdot(1+z)^{-1}\,. \qquad \text{(Eq.19)}$$

We define two coordinate system, which allows us to work with the vectors of coordinate bases $(\hat{x},\hat{y},\hat{z})$ and $(\hat{\theta},\hat{\Phi},\hat{\beta})$, and a rotation given by the angles shown in the figure 6:

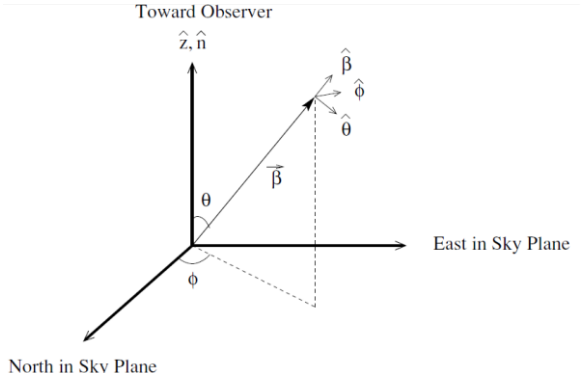


**Figure 6. Defined Coordinate systems.** ***From D. C. Homan (2009)*** **[20].**

Where the unit vector $\hat{\theta}$ tell us about the direction of increasing angle to the line of sight; $\bar{\beta}$ is the velocity vector at the rest frame and relates to the unit vector $\hat{\beta}$ as $\bar{\beta} = \beta\hat{\beta}$; $\Phi$ is the common polar angle in spherical coordinates (known as position angle in radio astronomical imaging terms), and unit vector $\hat{\Phi}$ is always perpendicular to the observed motion in the plane of the sky.

The accelerations in both reference frames are defined as (Blandford & Königl, 1979 [5]):

Rest frame: $$\frac{d\bar{\beta}}{dt} = \dot{\beta}\hat{\beta} + \beta\dot{\Phi}\sin\theta\,\hat{\Phi} + \beta\dot{\theta}\hat{\theta}\ , \qquad \text{(Eq.20)}$$

Observer frame: $$\frac{d\bar{\beta}_{app}}{dt_{obs}} = \left(1-\bar{\beta}\hat{n}\right)^{-3}\left[\left(1-\bar{\beta}\hat{n}\right)\frac{d\bar{\beta}}{dt} + \left(\frac{d\bar{\beta}}{dt}\hat{n}\right)\left(\bar{\beta}-\hat{n}\right)\right]. \qquad \text{(Eq.21)}$$

For observations it is useful to separate the apparent acceleration vector $\dot{\bar{\beta}}_{app}$ into two components $\dot{\beta}_{\parallel app}$ and $\dot{\beta}_{\perp app}$: the first one parallel to the velocity vector $\bar{\beta}_{app}$, and the second one perpendicular. Their equations are:

$$\frac{d\beta_{\parallel app}}{dt_{obs}} = \frac{d\bar{\beta}_{app}}{dt_{obs}}\cdot\hat{\beta}_{app} = \frac{\dot{\beta}\sin\theta+\beta\dot{\theta}(\cos\theta-\beta)}{(1-\beta\cos\theta)^3}, \qquad \text{(Eq.22)}$$

$$\frac{d\beta_{\perp app}}{dt_{obs}} = \frac{d\bar{\beta}_{app}}{dt_{obs}}\cdot\hat{\Phi} = \frac{\beta\dot{\Phi}\sin\theta}{(1-\beta\cos\theta)^2}. \qquad \text{(Eq.23)}$$

Parallel acceleration is associated to changes in apparent velocity, while perpendicular acceleration seems to be related to changes in apparent direction, that is, a non-radial motion. Changes in angle $\theta$ will directly affect to the parallel acceleration, as eq. 22 indicates. If we consider that apparent parallel acceleration is due entirely to changes in the value of the velocity $\beta$, then we get the simple relation:

$$\frac{\dot{\beta}_{\parallel app}}{\beta_{app}} = \frac{\dot{\mu}_{\parallel}}{\mu}(1+z) = \frac{\dot{\Gamma}}{\Gamma}\cdot\frac{\delta^2}{\beta^2}. \qquad \text{(Eq.24)}$$

The factor $\delta^2$ of eq. 24 tells us that small changes in the Doppler factor will considerably affect the apparent parallel acceleration $\dot{\beta}_{\parallel app}$. If we know the value of $\delta$, with equation 24 we can estimate the ratio $\dot{\Gamma}/\Gamma$ , useful when developing physical models of acceleration for the AGN.

Similarly, if we consider that $\dot{\beta}_{\perp app}$ is only dependent to changes in the direction of the source, we get:

$$\frac{\dot{\beta}_{\parallel app}}{\dot{\beta}_{\perp app}} = \frac{\beta\dot{\theta}}{\beta\dot{\Phi}\sin\dot{\theta}}\cdot\frac{\cos\theta-\beta}{1-\beta\cos\theta}. \qquad \text{(Eq.25)}$$

Other parameters useful when comparing observational data from different sources are the relative parallel and perpendicular accelerations $\dot{\eta}_{\parallel}$ and $\dot{\eta}_{\perp}$:

$$\dot{\eta}_{\parallel} = \frac{\dot{\beta}_{\parallel app}}{\beta_{app}} = (1+z)\frac{\dot{\mu}_{\parallel}}{\mu}, \qquad \text{(Eq.26)}$$

$$\dot{\eta}_{\perp} = \frac{\dot{\beta}_{\perp app}}{\beta_{app}} = (1+z)\frac{\dot{\mu}_{\perp}}{\mu}. \qquad \text{(Eq.27)}$$

About one half of all observed superluminal sources do not follow a straight trajectory (Homan et al. 2009 [20]), and do have bends and curvature.

### 3.4. Emission of light from a relativistic source

A source moving with relativistic speed experiences Doppler boosting, an effect described in *section 3.1*. But there also appears another consequence if a charged particle moves with $\beta \to c$: it radiates in preferred directions (following the synchrotron theory), and this will affect to the apparent luminosity measured by the observer.

If a particle is moving with low speed, it only emits radiation if its acceleration is non-zero. For this situation the power radiated per unit solid angle is governed by the Larmor's formula:

$$\frac{dE}{dt_p \cdot d\Omega} = \left(\frac{1}{4\pi}\right)^2 Z_0 q^2 \left|\dot{\bar{\beta}}\right|^2 \sin^2\theta\,. \qquad \text{(Eq.28)}$$

Where power radiated is the derivative of $E$ is with respect to the retarded time of the radiated signal $t_p$, $d\Omega$ is the differential solid angle, $Z_0$ is the impedance of the free space, $q$ is the charge of the particle and $\theta$ the angle between the particle velocity and the observer (equivalent to the line of sight angle). The radiation is maximum for an angle $\theta$ with a value of $\pi/2$, and is cancelled for directions parallel to $\bar{\beta}$. If the particle is now moving linearly with relativistic speeds, the power radiated per unit solid angle evolves as:

$$\frac{dE}{dt_p \cdot d\Omega} = \left(\frac{1}{4\pi}\right)^2 Z_0 q^2 \left|\dot{\bar{\beta}}\right|^2 \frac{\sin^2\theta}{(1-\beta\cos\theta)^5}. \qquad \text{(Eq.29)}$$

The representation of the power radiated depending on the angle $\theta$ between the velocity vector and the line of sight yields an interesting result:

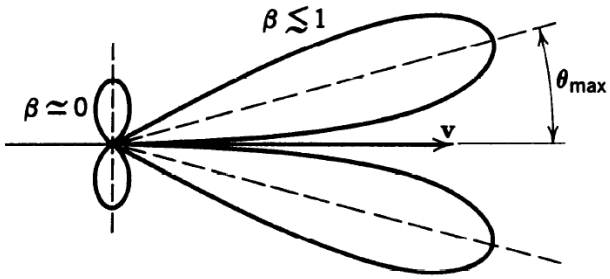


**Figure 7. Power radiated for relativistic and non-relativistic linear cases, depending on angle θ. Figures are not scaled, the relativistic cases has been reduced by a factor of 100 considering the same acceleration. *From: "Classical Electrodynamics" J.D. Jackson, 3rd Ed.* [21].**

There is a much more preferred direction for the radiation, with maximum at a defined angle $\theta_{max}$:

$$\theta_{max} = \cos^{-1}\left[\frac{1}{3\beta}\left(\sqrt{1+15\beta^2}-1\right)\right] \rightarrow \frac{1}{2\Gamma}. \qquad \text{(Eq.30)}$$

If we take the limit $\beta \ll 1$ in equation 29 the Larmor's formula is recovered. From eq. 30 the maximum value only depends on the velocity of the particle, and it decreases as $\beta$ becomes higher:

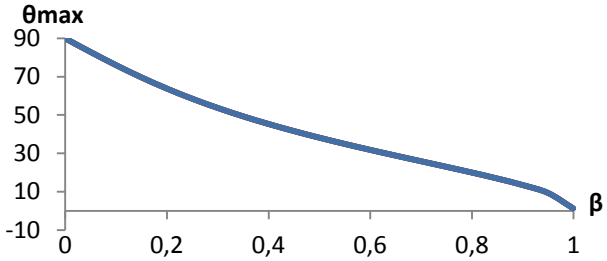


**Figure 8. $\theta_{max}$ as a function of velocity $\beta$.**

For a particle with circular trajectory and $\beta \rightarrow c$, the power radiated and its representation yield different results (where $\Phi$ is the angle between the acceleration vector and the line of sight):

$$\frac{dE}{dt_p \cdot d\Omega} = \left(\frac{1}{4\pi}\right)^2 Z_0 q^2 \left|\dot{\vec{\beta}}\right|^2 \frac{1}{(1-\beta\cos\theta)^3}\left[1 - \frac{\sin^2\theta\cos^2\Phi}{\Gamma^2(1-\beta\cos\theta)^2}\right]. \qquad \text{(Eq.31)}$$

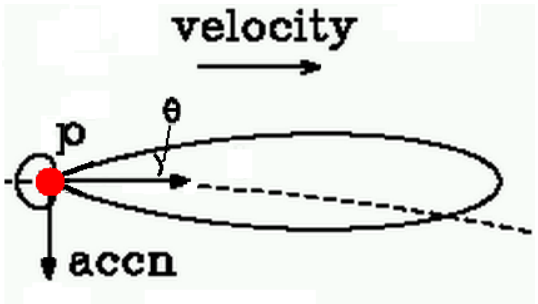


**Figure 9. Power radiated for relativistic particle with circular motion, depending on angle θ. *From C. Flynn: Synchrotron radiation notes* [22].**

In this case the maximum value of the power radiated is obtained when the angle $\theta = 0$, and for $\theta \sim 90°$ the radiation is non-zero.

For superluminal sources in astronomy, the apparent luminosity of the jet component will be directly affected by the angle $\theta$ in different ways. If the component has only linear acceleration, for an angle $\theta_{max}$ the radiation would be maximum and luminosity would be multiplied; for angles near that value apparent luminosity would also be increased; and for angles $\theta = 0$ there would be no radiation at all. If the feature of the jet only moves with perpendicular acceleration, the radiation would be high for small angles, maximum at $\theta = 0°$, and almost zero for the rest of the angles. And if the particle moves with both parallel and perpendicular accelerations, the power radiated by the jets would behave as a mixture of the two cases, and the behavior of apparent

luminosity would be rather difficult to determine, but generally we expect it would be powered at small angles.

## 4. Relations between parameters of the phenomenon

Before studying the connections between the basic parameters involved in superluminal motions we should clearly distinguish between the real motion followed by the feature and the projected trajectory measured in the plane of the sky. The real trajectory of the feature relative to the rest frame (with origin at the center of the host galaxy) can be linear (one-dimensional case) or curved (2D or 3D). What we observe is just a projection in 2D (in the plane of the sky) of the real motion: if the real trajectory is 1D, we also would observe a linear motion; if the component follows a 2D trajectory, we could see its projection as a linear trajectory (unlikely) or a curved one; and if the real motion is 3D, we will observe a 2D-trajectory in the plane of the sky.

About the involved parameters defining the jet motion and the other ones that we can measure at observations, the basic jet properties are the velocity $\beta$, the intrinsic luminosity $L_{int}$ and the Lorentz factor Γ. The parameters we can quantify via observations are the apparent transverse speed $\beta_{app}$, the apparent luminosity $L_{app}$ ($L_{app} = L_{int} \cdot \delta^n$) and consequently the Doppler factor $\delta$ (see *e.g.*, Ros *et al.* 2008 [23]). This is summarized in table 1. In addition to these parameters, estimates of the perpendicular and parallel apparent accelerations $\dot{\beta}_{\perp\, app}$ and $\dot{\beta}_{\parallel app}$ could also be obtained.

| Basic jet properties | | What we observe | |
|---|---|---|---|
| Jet Plasma Bulk Velocity | $\beta = v/c$[a] | Apparent Speed | $\beta_{\rm app} = \beta \sin\theta/(1-\beta\cos\theta)$[b] |
| Intrinsic Luminosity | $L_{\rm int}$ | Luminosity | $L_{\rm obs} = L_{\rm int} \times \delta^{n}$[c] |
| Intrinsic Brightness Temperature | $T_{\rm b,int}$ | Brightness Temperature | $T_{\rm b,obs} = T_{\rm b,int} \times \delta$ |
| Bulk Lorentz Factor | $\Gamma = (1-\beta^2)^{-1/2}$ | Doppler Beaming | $\delta = \Gamma^{-1}(1-\beta\cos\theta)^{-1}$ |

[a] $v$ is the speed of the plasma, and $c$ is the light speed.
[b] $\theta$ is the viewing angle, notice that $\beta_{\rm app,max} \approx \Gamma$when $\theta = \Gamma^{-1}$.
[c] $n$ depends on the jet geometry and is typically in the range between 2 and 3.

**Table 1. Intrinsic and observed parameters of jets. *From E. Ros* [23].**

In this section of the paper we describe the relations between the parameters involved in the motion, working with numerical values when given certain input parameters. We will focus on a real one-dimensional motion of the component, and afterwards we will provide some hints on how to generalize to the three-dimensional case for a further insight of superluminal motion.

### 4.1. One-dimensional case (*1D*)

We consider here an object with linear motion, that is, it can't turn or change its direction. The object is just allowed to accelerate in the direction of the movement and therefore the observer will measure a projected linear trajectory.

The parameters needed for describing this case are: the apparent velocity of the object as seen from an observer outside the host galaxy $\beta_{app}$, the velocity of the component at the rest frame $\beta$, the angle $\theta$ between the line of sight and the direction of the motion, the Lorentz factor Γ and the Doppler boosting factor $\delta$. The critical velocity $\beta_{crit}$ is also a useful quantity in superluminal motion, so it will be included in this analysis.

We see from equation 14 that different combinations of $\beta$ and $\theta$ could yield the same apparent velocity $\beta_{app}$. Therefore there exists degeneracy, and for avoiding it we should determine at least two of those parameters.

The method used in this analysis goes as follows: we first consider a low value of the apparent velocity $\beta_{app}$ (but higher than the unity to achieve superluminal motion), and from it we find out the possible set of values for the rest of the parameters $(\beta, \theta, \Gamma, \delta, \beta_{crit})$. Once we have obtained the complete set of possible values, we increase the value of the apparent velocity $\beta_{app}$, repeating the calculation of the other parameters. This procedure goes on until the value of $\beta_{app}$ reaches the maximum observed at present time, approximately $\beta_{app} \sim 50$ (Lister *et al*. 2009 [2]).

To obtain all the possible combinations for each $\beta_{app}$ considered, we give different values to $\theta$, and with those two parameters it is straightforward to get the rest using equations (2), (6), (14) and (15) (see tables 2 and 3).

| $\beta_{app}$ = 2 | $\Theta_{lim}$=53º |
|---|---|

| **θ [°]** | 0,01 | 1 | 5 | 10 | 15 | 20 | 30 | 45 | 60 | 90 |
|---|---|---|---|---|---|---|---|---|---|---|
| **β** | 1 | 0,99 | 0,96 | 0,93 | 0,91 | 0,90 | 0,90 | 0,94 | 1,1 | 2 |
| **Γ** | 76 | 7,7 | 3,7 | 2,8 | 2,5 | 2,3 | 2,3 | 3 | - | - |
| **$\beta_{crit}$** | 76 | 7,6 | 3,5 | 2,6 | 2,2 | 2,1 | 2,0 | 2,8 | - | - |
| **δ** | 150 | 15 | 6,5 | 4,4 | 3,5 | 2,8 | 2,0 | 1 | - | - |

| $\beta_{app}$ = 5 | $\Theta_{lim}$=23º |
|---|---|

| **θ [°]** | 0,01 | 1 | 5 | 10 | 15 | 20 | 30 | 45 | 60 | 90 |
|---|---|---|---|---|---|---|---|---|---|---|
| **β** | 1 | 1,0 | 0,99 | 0,98 | 0,98 | 0,99 | 1,0 | 1,2 | 1,5 | 5 |
| **Γ** | 120 | 12 | 6,1 | 5,1 | 5,4 | 7,9 | - | - | - | - |
| **$\beta_{crit}$** | 120 | 12 | 6,0 | 5,0 | 5,3 | 7,8 | - | - | - | - |
| **δ** | 240 | 23 | 9,5 | 5,7 | 3,6 | 1,9 | - | - | - | - |

**Tables 2 and 3. For each table $\beta_{app}$ is assumed to be 2 and 5 respectively. The rest of the parameters are calculated giving different values to angle θ. For angles higher than $\theta_{lim}$ the results are non-physical (indicated by red color for β values).**

Tables 2 and 3 are examples of the employed method, with $\beta_{app}$ values of 2 and 5 respectively. These tables show explicitly that this procedure brings out non-physical states, since for high enough values of angle $\theta$ the intrinsic velocity $\beta$ becomes higher than speed of light, violating the fundamental principle of special relativity. Therefore we deduce that the admitted values of the angle $\theta$ go from zero to an upper limit (denoted as $\theta_{lim}$):

$$\theta \in ]0, \theta_{lim}[ \,. \qquad \text{(Eq.32)}$$

This upper limit is inversely dependent on the apparent velocity $\beta_{app}$. In other words, the admitted interval decreases as $\beta_{app}$ grows. To deduce the limiting value $\theta_{lim}$ we work with eq. 14, demanding to $\beta$ to be lower than unity. We get:

$$\theta_{lim} = 2 \cdot \arctan\left(\frac{1}{\beta_{app}}\right). \qquad \text{(Eq.33)}$$

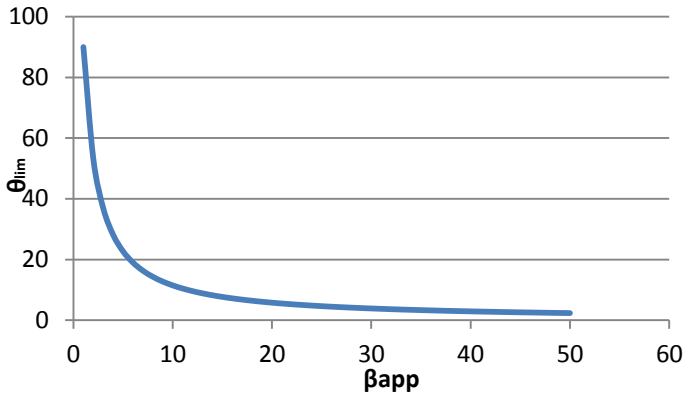


Figure 10. Upper limit of angle θ as a function of $\beta_{app}$.

We can represent all the parameters as functions of angle $\theta$ (figures 11, 12, 13 and 14). In the figures, each curved line represents the evolution of one parameter with constant value of $\beta_{app}$. These lines of constant apparent velocities are limited to $\theta_{lim}$ for all the parameters.

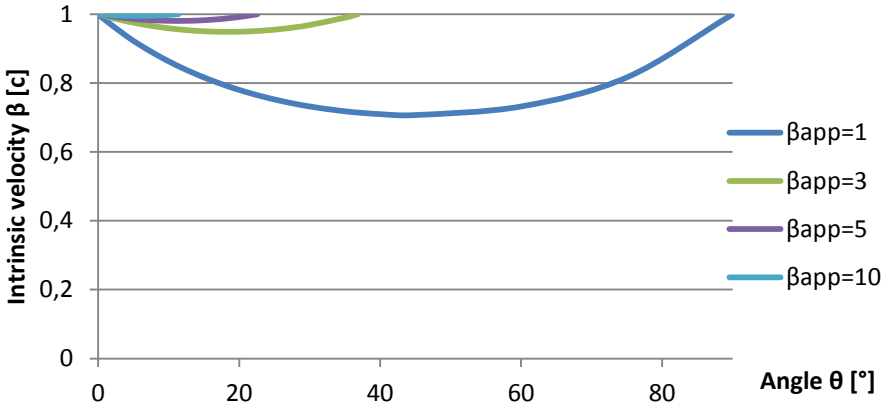


Figure 11. Representation of the intrinsic velocity β as a function of angle θ, for different values of $\beta_{app}$.

The graph of the intrinsic velocity shows that contours of constant $\beta_{app}$ follow a parabola, with maximum values at angles 0º and at $\theta = \theta_{lim}$, and a minimal placed at the middle of the interval. If we increase the values of $\beta_{app}$, we get smaller parabolas at higher $\beta$. Degeneracy is also visible in figure 11 since two different values of $\theta$ could be obtained by two different combinations of $\beta$ and $\beta_{app}$.

A similar trend is followed by the parameters $\Gamma, \beta_{crit}$ and $\delta$: these are directly proportional to $\beta_{app}$.

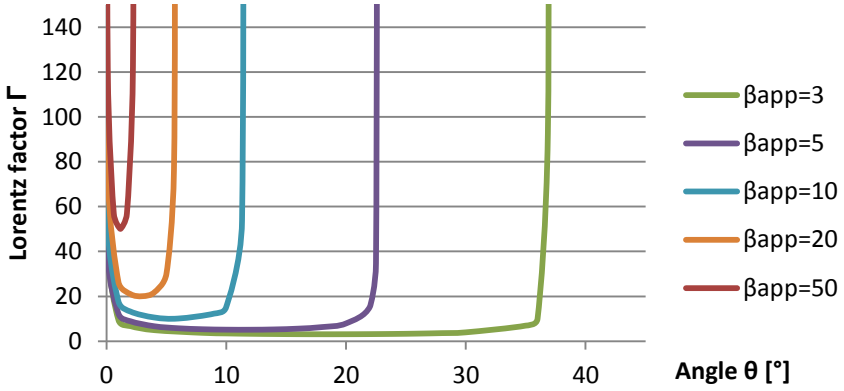


Figure 12. Lorentz factor as a function of angle θ.

Lorentz factor behaves slightly different: it also grows proportional to $\beta_{app}$, but now Γ tends to infinite for an angle going to 0 or $\theta_{lim}$.

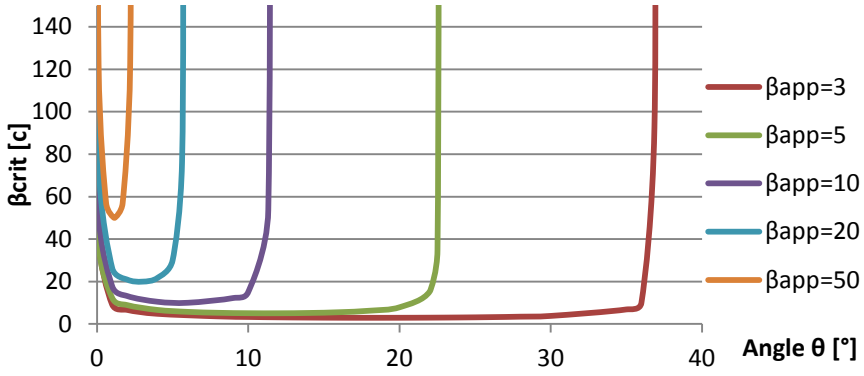


Figure 13. $\beta_{crit}$-θ diagram.

The evolution of $\beta_{crit}$ is basically equal to that of the Lorentz factor. Both are equivalent for high values, but at small values, $\beta_{crit}$ becomes smaller than Γ.

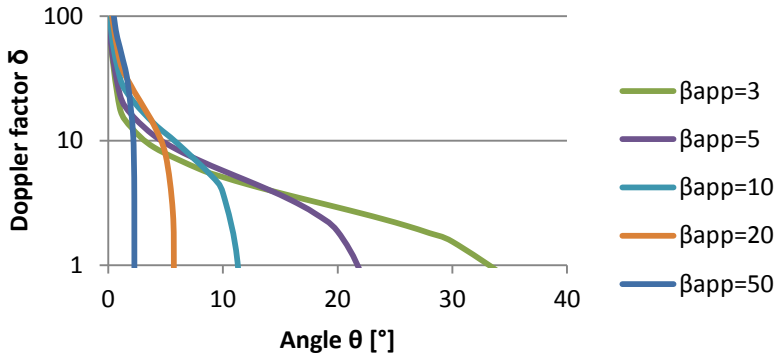


Figure 14. Doppler boosting factor as a function of angle θ. Vertical axis is in logarithmic scale.

Doppler factor evolves exponentially, tending to 0 for angles near $\theta_{lim}$, and going to $+\infty$ if angle approaches to zero. For a given $\theta$, Doppler factor increases proportional to $\beta_{app}$.

Relationships between parameters and the associated degeneracy can be seen properly if we represent $\delta$ and $\theta$ as contours of constant value depending on the parameters $\beta_{app}$ and $\delta$ (see figure 15). If for example we know the value of $\beta_{app}$, from figure 15 we could restrict the possible values for the rest of the parameters.

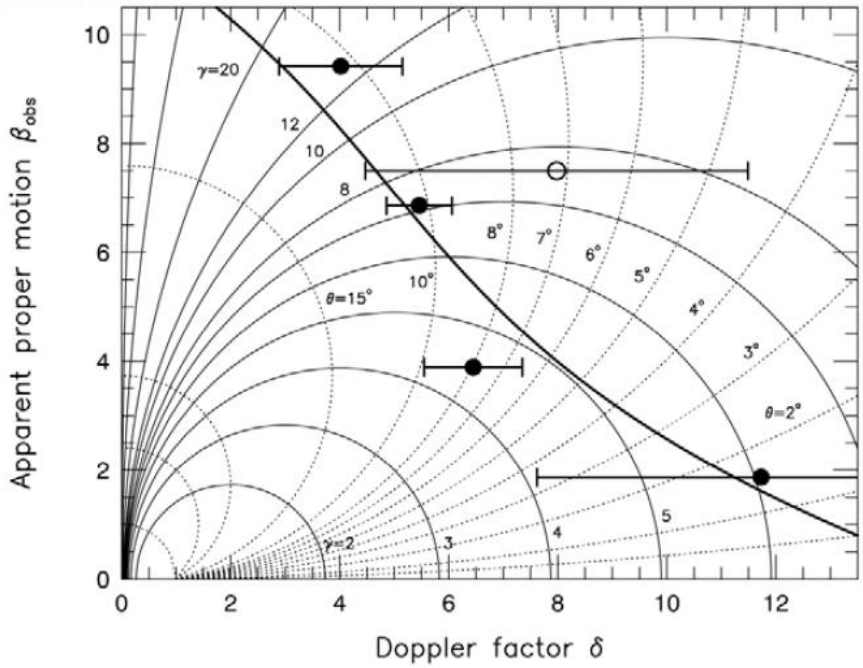


**Figure 15. Contour of constant Lorentz factor Γ and angle θ, being the axis the two geometric observables $\beta_{app}$ and Doppler factor $\delta$ The curved line derived form observations shows for a certain value of $\beta_{app}$ the common values measured of the other parameters. *From Encyclopedia of Astronomy and Astrophysics* [24].**

From figure 15 we can also deduce the degeneracy between parameters, as for given values of $\beta_{app}$ and Γ (represented as $\gamma$ in the figure), two different values of the Doppler factor $\delta$ are admitted. Similarly, for known values of $\delta$ and $\theta$ there are two allowed values of $\beta_{app}$. This degeneracy would be broken if we know $\beta_{app}$ and $\delta$: then the parameters Γ and $\theta$ are univocally determined. Indeed in observations the tipical measured parameters are $\beta_{app}$ (as explained in *section 2*) and $\delta$ (from apparent luminosity), avoiding this degeneracy.

### 4.2. Three-dimensional case (*3D*)

This is the general situation where the superluminal object of the jet is allowed to turn and change the direction of its motion in a 3D-space, hence we would observe a projected 2D trajectory at the sky plane. Current observations suggest that this case is quite common for most of the studied superluminal objects: about 50% of the objects appear to move in variable directions depending on their relative position to the center of the jet (Homan *et al*. 2009 [20]).

A complete study of this case implies an extensive simulation with many parameters that can affect both the intrinsic trajectory followed by the component and the apparent

parameters measured by the observer, and therefore the 3D-case surpasses the scope of this work.

Allowing the component to move in every direction is equivalent to saying that the derivatives of the angle $\theta$ and of the azimuthal angle $\Phi$ could be non-zero, that is to say, $\dot{\theta} \neq 0$ and $\dot{\Phi} \neq 0$. If just one of these angular derivatives are non-zero we would be talking about a real two-dimensional motion. The one-dimensional case takes place when both derivatives are zero. Based on the 1D analysis we could use the obtained sets of parameters $\{\beta_{app}, \beta, \theta, \Gamma, \delta, \beta_{crit}\}$ and give different values to $\dot{\theta}$ and $\dot{\Phi}$ in addition. From all these input parameters we could calculate the apparent perpendicular acceleration $\dot{\beta}_{\perp\, app}$ with eq. 23, the apparent parallel acceleration $\dot{\beta}_{\parallel app}$ (eq. 25), and therefore the derivative of the Lorentz factor $\dot{\Gamma}$ (eq. 24), the intrinsic acceleration $\dot{\beta}$ (eq. 22) and the acceleration vector $\dot{\vec{\beta}}$ of the component (eq. 20).

But this becomes a complicated simulation with many parameters that can change its value, so this method is not employed. Instead, what simulations usually do is to assume a certain trajectory (typically a helix or a Kelvin-Helmholtz type), and then try giving different values to the main parameters $\beta$, $\theta$ and geometric parameters of the chosen trajectory (as the angle of aperture $\psi$ for a helix), and deduce the rest from them.

As a first approach we could assume parameters to be constant in time, but a more accurate analysis would require some parameters to change in time, firstly the velocity $\beta(t)$, and subsequently $\theta(t)$ or/and $\psi(t)$.

## 5. Deductions from observations

In this part we summarize selected findings and discoveries made by observers and different research groups about the kinematics and other physical characteristics of the AGN.

First of all, an observation of a superluminal source requires the identification of the two main parts, the core and the jet. For doing this, the core usually appears as a compact component located at one end of the whole source, and presents a flat radio spectrum (considering a flat spectrum when $\alpha > -0{,}5$, and $\alpha$ being the factor from relation $S_\nu \propto \nu^\alpha$), meanwhile the jets have steeper spectrum and generally spread. But their distinction is not always easy because the two parts could not present many differences. Sometimes difficulties rise from the identification of the components from one epoch to another (*e.g.*, Blandford 1987 [25]). Components with fast angular speeds, a high rate of new features at small time intervals, small jets compared to the resolution, or near-stationary components usually are the most problematic issues that can make impossible the determination of the kinematic properties of the jet.

In a few observed AGN the two jets and the core are distinguished (see figure 16), these are named as two-sided jets, *e.g.*, compact symmetric objects or nearby galaxies such as NGC1052 (*e.g.*, Vermeulen *et al.* 2003 [26]; Kadler *et al.* 2004 [27]). This happens when the Doppler boosting (or de-boosting) factor is small for each jet, and that occurs if the angle $\theta$ between the line of sight and the motion's direction is near 90º. The data from MOJAVE suggests that the observed two-sided jets are mostly low-luminosity radio galaxies.

Once the core and the jet features are uniquely identified, observers can quantify different parameters involved in superluminal motions, mainly by measuring positions and apparent luminosities and knowing (from another independent method) the redshift *z* of the source.

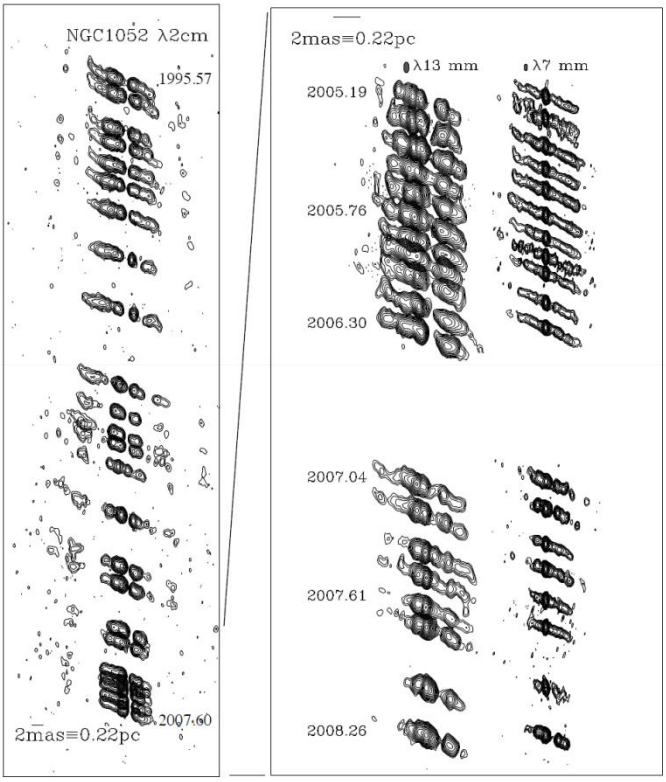


**Figure 16. VLBA images of NGC1052. The left panel shows contours at 2cm over a decade from MOJAVE survey. The right panel represents the same galaxy at high frequencies (at wavelengths 13mm and 7mm respectively), evaluated since 2005.** ***From E.Ros and M. Kadler (2008)*** **[28].**

## 5.1. Ongoing surveys

Since the end of 1980s different groups have been searching for superluminal motions in AGN with the aim of getting a better understanding of the relativistic flows (bulk/pattern speeds…).

In the 1990s VLBI techniques were substantially improved, and observations of large amounts of AGN with the determination of different characteristics of the sources became routinely possible, especially since the construction of the VLBA, dedicated full-time to VLBI observations (see Napier *et al.*, 1994 [29]).

The tendency is to unify the enormous amount of data that exists nowadays in the field, so VLBI networks spread in the northern and southern hemispheres trying to work together, coordinating a global network that brings out an improvement in the resolution and in quality of the observations. At the present time the main ongoing surveys work in collaboration, but each one with slightly different purposes or objectives.

Surveys observing to short wavelengths often need to be more frequently sampled, since they access to the (elsewhere self-absorbed) innermost part of the jet and "see"

more compact and more rapidly moving features. Therefore those have to focus on small samples with high luminosity. On the contrary, longer wavelengths have better brightness sensitivity so trajectories can be obtained for longer distances, but the angular resolution results poorer.

The most important surveys taking place nowadays are: VIPS, Boston University Blazar Program, MOJAVE and TANAMI (Ros 2011 [30]).

- The first one, named VLBA Imaging and Polarimetry Survey works at 5GHz yielded a complete and accurate analysis of 1127 sources, including polarimetry but only one observation epoch, and concluded in the late 2000s (see Hemboldt *et al*. 2007 [31]; Linford *et al*. 2011 [32]).

- The BU Blazar Group focuses on a few sources only, but with a monthly sampling at 43GHz since 2007 (Marscher *et al*. 2011 [33]).

- MOJAVE was started in 1994 as the VLBA 2cm Survey project and was devoted to the observation of bright AGN at sub-parsec scales. Since 2002 the survey was renamed as MOJAVE (Monitoring Of Jets in Active galactic nuclei with VLBA Experiments) and at the present time it is devoted to the study at 15GHz of over 300 sources, including a statistically complete sub-set of 135 sources above -30º. With its long-term sampling, it yields high-quality jet motions including dual polarization (Zensus *et al*. 2002 [34], Lister *et al.*, 2009 [2]).

- Since 2007 the TANAMI (Tracking Active Galactic Nuclei with Austral Miliarcsecond Interferometry [35]) project complements to MOJAVE and collects data of sources at declination below -30º (Ohja *et al.*, 2010 [36]).

- There also exist less significant groups and individual studies. In general those would complement and help the main surveys named above.

| Program | $\lambda$ | $N_{sources}$ | $N_{epochs}$ [a] | Time |
|---|---|---|---|---|
| GMVA 3mm | 3 mm | 121 | 2 | 2004- |
| **Boston Univ.** | 7 mm | 35 | 50 | 2007- |
| TeV Sample | 7 mm [b] | 7 | 5 | 2006- |
| **MOJAVE/2 cm Survey** | 2 cm | 300 | 20 | 1994- |
| Bologna low-$z$ | 2/3.6 cm | 42 | 2 | 2010- |
| **TANAMI** | 1.3/3.6 cm | 80 | 5 | 2008- |
| **VIPS** | 6 cm | 1127 | 1 | 2007 |
| VIPS subsample | 6 cm | 100 | 2 | 2010- |
| CJF | 6 cm | 293 | 3 | 1990s |
| ICRF | 3.6/13 cm | 500 | 10 | 1990s |
| VCS | 3.6/13 cm | 3400 | 1 | 1990s |

[a] Typical number of epochs per source
[b] Also including $\lambda$1.3 cm & $\lambda$3.6 cm

**Figure 17. Main ongoing VLBI surveys.** ***From E. Ros (2011)*** **[30].**

For a better insight of the physics of radio galaxies and their behavior, these superluminal surveys have to be complemented with surveys on other fields, as for example, on $\gamma$-ray surveys. This is the case of the *Fermi Gamma-ray Space Telescope* (FGST) that since 2008 observes any $\gamma$-ray source of the sky every few hours. This

telescope and others should complement the ongoing surveys on superluminal motion for acquiring better understanding of AGN as a whole.

### 5.2. Apparent velocities

From MOJAVE data, about one third of all the studied sources show changes in speed, or equivalently, one third moves with non-zero acceleration. Plotting the time evolution of the separation from the core of each component (as in figure 18) clearly shows the time dependency of the apparent velocity, in such a way that curvatures imply variations in $\beta_{app}$.

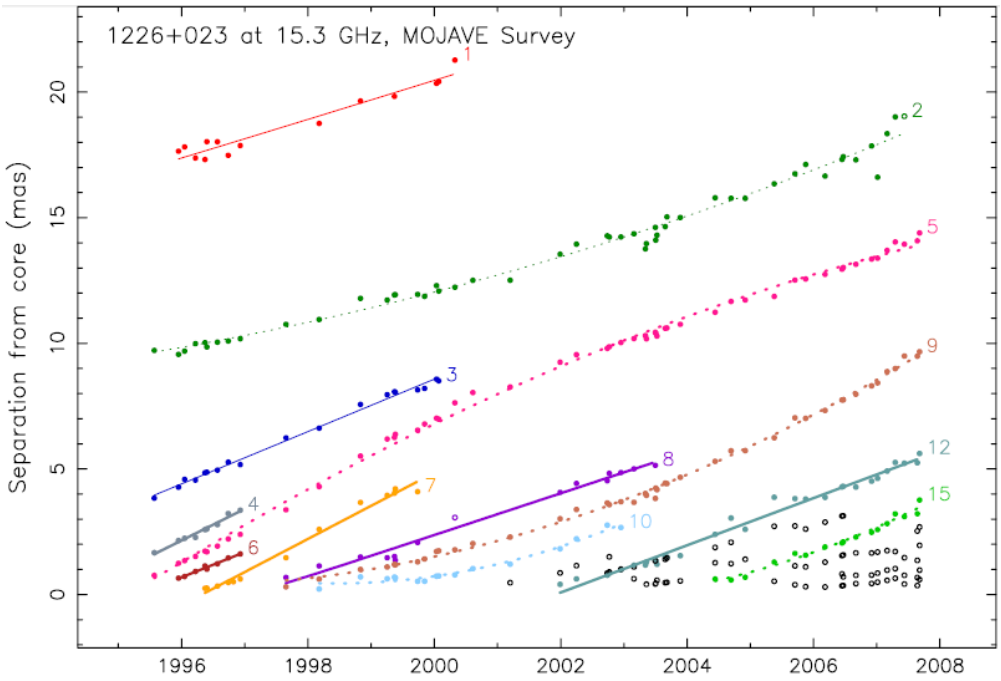


**Figure 18. Representations of the separation from the core as a function of time. The graph shows different features for the galaxy 1226+023, and clearly indicates changes in apparent velocity. Observed at 15,3GHz by *MOJAVE survey (Lister et al.* [2]*).***

In general, there is a trend that the most luminous sources have the fastest apparent velocities (Cohen *et al*. 2007 [37]; Britzen *et al*. 2008 [38]). Usually it is defined a characteristic speed of a jet as the maximum apparent velocity measured from all the components of that jet.

The distribution of the observed velocity of all the studied sources at MOJAVE is peaked around 10$c$, and the maximum apparent velocity observed so far is ~50$c$ (see figure 19). Distinguishing between different AGN types, quasars show higher apparent velocities than BL Lacertae and other radio galaxies (Ros 2008 [23]).

In some studies the observed trend shows that speed is higher at larger distances from the core (Homan *et al*. 2001 [39]; Piner *et al*. 2006 [40]; Britzen *et al*. 2008 [38]); but there are other studies which suggest exactly the opposite, a tendency for higher velocities at smaller distances from the jet (Kellerman 2004 [41]). Other observations yield behaviors where firstly the component velocity grows, then there is a pronounced

minimum at a certain distance from the core, and finally it grows again (Zensus *et al*. 1997 [42]).

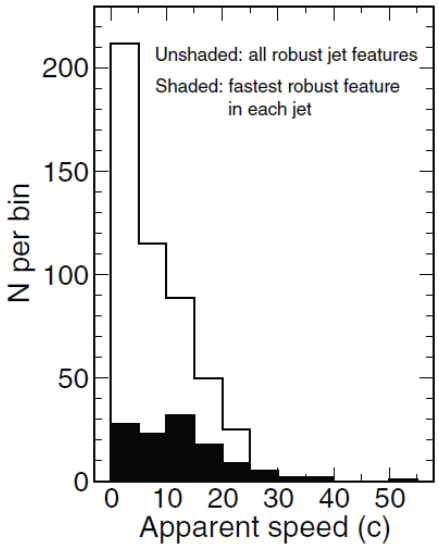


**Figure 19. Distribution of $\beta_{app}$ for 502 jet features.** ***From Lister et al., 2009*** **[2].**

### 5.3. Parallel and perpendicular accelerations

Parallel accelerations, which are related to variations in apparent speed, tend to be larger than perpendicular accelerations, which represent changes in the direction of the motion. Non-radial motion happens in almost one half of the studied AGN, and it is directly caused by accelerations in a direction perpendicular to the motion (Homan *et al*. 2009 [20]). Non linear motion of jet's components in such a high percentage is used as an argument against the alternative hypothesis for which superluminal components of the jets are in fact moving plasmons (Zensus *et al*. 2007 [43]).

Figure 20 shows three examples of different AGN components having parallel and perpendicular accelerations. The first column displays the general observed contour of the galaxies; the second one shows the projected trajectories of the components in the sky plane, diagnosing the presence of non-radial motion and therefore of perpendicular accelerations. The last column represents the relative distance of each component from its galaxy core, indicating the existence of parallel accelerations if the trajectory is curved. The plots of the 0333+321 component suggest it has both parallel and perpendicular acceleration; the 1222+216 component seems to evolve with just perpendicular acceleration; while the 1226+023 feature only shows parallel acceleration, implying changes in apparent velocity.

From MOJAVE data (Homan *et al*. 2009 [20]), approximately one third of the studied components have a relatively high parallel acceleration, while one fifth would have high perpendicular acceleration. High acceleration is considered if components have the ratio $\dot{\beta}_{app}/\beta_{app} > 0.1$.

There seems to be a trend that bindings of the jet are more pronounced in core-dominated sources than in jet-dominated ones. Another interesting point is that

apparently trajectories near the core differ more significantly than far from the core, where trajectories become similar (Zensus *et al*. 1997 [42]).

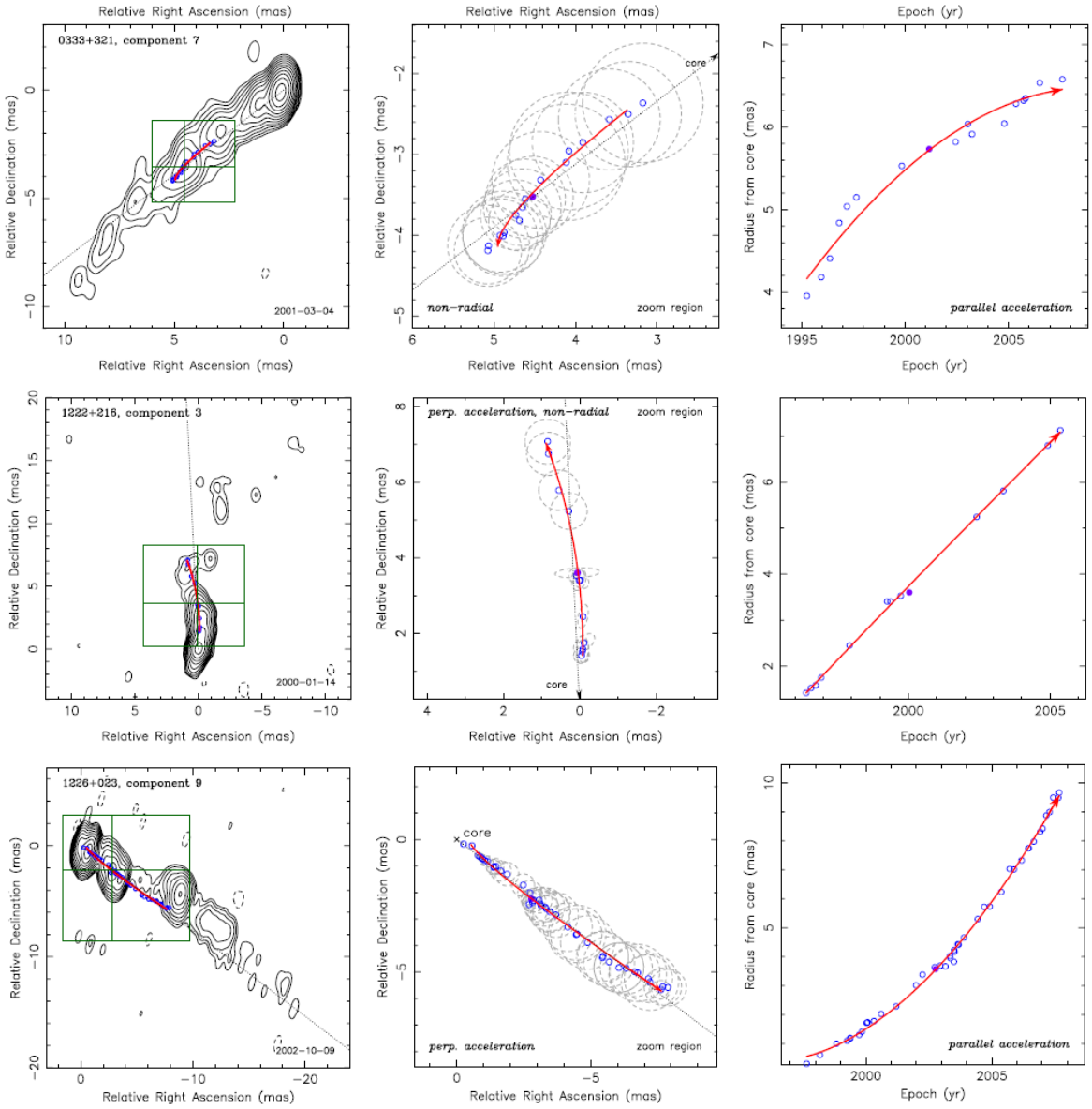


**Figure 20. Plots of component trajectories in 0333+321, 1222+216 and 3C 273 (each component per row). The left-hand graph shows a contour image for one epoch, the position of the component for different epochs, a radial line from the jet core to the component position at the same epoch of the contour image, and a fit trajectory of the component. The middle graph is a zoomed view of the component's position at the sky plane., and the right-hand graph shows the radial distance of the component from the core of its galaxy. *From Homan et al., 2009* [20].**

Measured accelerations seem to be related to changes in the Lorentz factor more than to changes in the angle to the line of sight (Homan *et. al*. 2009 [20]). This is supported by the fact that measurement of parallel accelerations bring out larger magnitudes than for perpendicular accelerations.

### 5.4. The flow's path

A very important issue to be clarified is if each component follows the same path within the jet or if there is no relation. Some observations seem to confirm the existence of such a jet path (as for example in quasar 3C 273); but on the other hand there are other cases where this is not obeyed at all (as in 3C 279).

What is usually observed, is a trend where trajectories seems to be curved and quasiperiodic (Camenzind & Krockenberger 1992 [44], Hardee *et al.*, 1987 [45], Königl & Choudhuri 1985 [46], Camenzind *et al.*, 1986 [47], Qian *et al* 1991 [48], 1996 [49]), in a way that the jet's path is significantly followed by each feature, but with small variations. This trend is defined as helical motion of the jets. Sometimes an observed trend for different components of the same quasar is that at short projected distances from the core their trajectories differ significantly, while for larger distances they seems to follow similar paths, as in 3C 345 (Zensus *et al*. 1997 [42]), or in 4C 39.25 (Alberdi *et al.* 1997 [50]).

There are observations of some AGN where jet components have different apparent velocities, indicating that the motion of the features could not depend on the flow. Due to the high percentage of AGN with jets evolving with non-radial motion, it has been suggested that the features can in fact change their direction once they have been ejected from the core. On the other hand, most of the components with non-radial motion seem to move in a direction which will tend to make them better aligned with the downstream emission (Homan *et al*. 2009 [20]), suggesting that it is possible to define a path which approximately guides the motion of the components.

It has been reported the existence of some blazars ejecting components at different angles. In these cases, the observed trajectories of the features could seem to be curved, even though those could be in fact linear (Homan *et al*. 2012 [51]).

There seems to be a correlation between the jet speeds of the AGN and their $\gamma$-ray emission (Lister *et al*. 2009 [2]; Kovalev *et al*. 2009 [52]). AGN with $\gamma$-ray emission seems to have faster jets than AGN without $\gamma$-ray activity (Kellermann *et al*. 2004 [41]). For getting a better comprehension of the whole physics involved in AGN, the VLBI surveys have to be related to $\gamma$-ray measurements for every studied source. Proceeding in this way it should be possible to understand all the mechanisms that take place in an active galaxy, from the way the core ejects matter at high velocities, to all the kinematics and the behavior of the jets.

### 5.5. Microquasars

Although most of the superluminal sources are extragalactic quasars or AGN, in last decade there have been reported some objects inside our Milky Way that also develop superluminal motion (Unwin *et al*. 2001 [24]).

The definition of microquasar is a stellar-mass object inside our galaxy that behaves like a quasar. For these sources superluminal motion has also been reported: the first time in 1994 by Mirabel and Rodríguez with the discovery of the microquasar GRS 1915+105. This source is believed to be a binary star only a few times the mass of the Sun, in which one of the components would be a black hole pulling material at relativistic speeds from the smaller component. Since then, other microquasars have

been discovered (Paredes *et al.* 2006 [53]), V4641 Sagittarii being the closest microquasar to the Sun found to date, at about 500pc of distance [54].

## 6. Conclusions

- Superluminal motion in astronomy happens when an object is measured to move with an apparent velocity higher than speed of light, suggesting a violation of the special relativity principles. This phenomenon is an illusion due to the relative velocity between the observer frame and the rest frame of the moving object, and can be explained with simple geometry.

- This event takes place in AGN for extragalactic sources, but also in microquasars in our own galaxy. The phenomenon was predicted in 1966 and discovered some years later. While observed (or apparent) velocity $\beta_{app}$ of the component can easily exceed the speed of light $c$, the intrinsic velocity $\beta$ in the rest frame will always be lower than $c$.

- AGN are formed by a central core and two jets. In the central core there is a black hole attracting material from a surrounding accretion disk, and consequently material at relativistic speed is ejected from the core, creating the observed jets.

- The study of the trajectories of the superluminal jets can help to the understanding of all the physics and kinematics related to AGN, and with this aim superluminal sources are extensively studied by different surveys and observers.

- The observed motions of the components show curvatures and changes in velocity. Curved trajectories are due to observed perpendicular acceleration, while variations in velocity are due to changes in apparent parallel acceleration.

- The parameters needed for studying superluminal components are mainly $\beta_{app}, \theta, \beta, \Gamma$ and $\beta_{crit}$. From observations we can measure $\beta_{app}$ and $\delta$, and the rest can be derived from those two.

- Doppler boosting factor $\delta$ largely affects the apparent luminosity of the source $L_{app} = L_{intrinsic} \cdot \delta^n$. Usually small angles $\theta$ imply large $\delta$ and therefore the apparent luminosity is powered.

- For the same angle $\theta$, the parameters $\beta, \Gamma, \beta_{crit}$ and $\delta$ are directly dependent on the value of apparent velocity $\beta_{app}$. For avoiding the degeneracy we should measure $\beta_{app}$ and $\delta$.

- So far it is not clear if the jet components follow a well defined path or if each one follows an independent trajectory.

# Conclusiones

- El movimiento superlumínico en astronomía sucede cuando un objeto se observa que posee una velocidad aparente mayor que la velocidad de la luz, lo que implica un incumplimiento del principio de relatividad especial. Este hecho es una ilusión debida a la velocidad relativa entre los sistemas de referencia asociados al observador y al objeto, y puede ser explicado con sencilla geometría.

- Este fenómeno tiene lugar en AGN para fuentes extragalácticas, pero también en microcuásares en nuestra propia galaxia. Fue predicho en 1966 y descubierto posteriormente. Mientras que la velocidad observada (o aparente) $\beta_{ap}$ puede ser ampliamente superior a $c$, la velocidad intrínseca $\beta$ del objeto nunca superará dicho límite.

- AGN están formados por por una región central y dos "jets". En la región central se encuentra un agujero negro que atrae material procedente de un disco de acreción situado alrededor del agujero negro. En consecuencia el material es expulsado a velocidades relativistas desde el centro, creando los jets que usualmente se observan.

- El estudio de las trayectorias de los jets superlumínicos puede servir para comprender la física de los AGN, y con este propósito distintos grupos de investigación estudian extensivamente cualquier fuente superlumínica.

- Los movimientos observados de las componentes muestran curvaturas y cambios en la velocidad. Trayectorias curvadas se asocian a la aceleración perpendicular medida, mientras que variaciones en la velocidad son debidas a la aceleración paralela observada.

- Los parámetros que se necesitan para el estudio del movimiento superlumínico son principalmente $\beta_{ap}, \theta, \beta, \Gamma$ y $\beta_{crít}$. De las observaciones se pueden medir $\beta_{ap}$ y $\delta$, mientras que el resto se derivan de estas dos.

- El factor de Doppler $\delta$ afecta en gran medida la luminosidad aparente de la fuente $L_{ap} = L_{intrínsica} \cdot \delta^n$. Generalmente pequeños ángulos $\theta$ implican un valor elevado de $\delta$, y por tanto la luminosidad aparente se ve multiplicada.

- Para un valor concreto del ángulo $\theta$, los parámetros $\beta, \Gamma, \beta_{crít}$ y $\delta$ crecen proporcionalmente al calor de la velocidad aparente. Para evitar la degeneración es suficiente con medir $\beta_{ap}$ y $\delta$.

- Hasta el momento aún no está claro si las componentes de los jets siguen un camino bien definido o si cada cual sigue una trayectoria independiente.

# 7. References

[1] R A Laing et al., "Faster than light: superluminal motion and light echoes", Physics Education (UK), Vol. 32, No. 1, p. 30 - 34.
[2] M. L. Lister, M. H. Cohen, D. C. Homan, M. Kadler, K. I. Kellermann, Y. Y. Kovalev, E. Ros, T. Savolainen, & J. A. Zensus, *Astronomical Journal*, 138: 1874-1892 (2009).
[3] B. F. Burke, F. Graham-Smith, "An Introduction to Radio Astronomy", Cambridge, 3rd Edition.
[4] J. D. Kraus, "Radio Astronomy", Cygnus-Quasar Books, 1984.
[5] R. D. Blandford, & A. Königl, 1979, ApJ, 232, 34.
[6] Aurore Simonnet, Sonoma State University, http://www.nasa.gov/.
[7] M. J. Rees (1966), *Nature*, 211, 468.
[8] W. A. Dent (1965), *Science*, 148, 1458.
[9] J. Gubbay, A. J. Legg, D. S. Robertson, A. T. Moffet, R. D. Ekers & B. Seidel (1969), *Nature*, 224, 1094.
[10] A. T. Moffet, J. Gubbay, D. S. Robertson & A. J. Legg (1972), in '*IAU Sympomum 119, Quasars'*, ed. G. Swarup and V. K. Kapahi (Dordrecht: Reidel), p. 228.
[11] I. F. Mirabel &L. F. Rodriguez (1994), *Nature* 371 46.
[12] A. P. Marscher, 1998 "The blazar paradigm" ASP Conference Series 144 (San Francisco, CA: ASP) pp25–32.
[13] M. Kadler, E. Ros, M. Perucho, Y. Y. Kovalev, D. C. Homan, I. Agudo, K. I. Kellermann, M. F. Aller, H. D. Aller, M. L. Lister, J. A. Zensus, NRAO/AUI and C. Fromm, Max-Planck-Institut für Radioastronomie.
[14] R.A. Laing, Physics Education (UK), Vol. 32, No. 1, p. 30 – 34.
[15] D.F. Falla & M.J. Floyd, Eur. J. Phys. 23 (2002), 69-81.
[16] D. L. Meier, S. Koide, & Y. Uchida, 2001, Science, 291, 84.
[17] R.C. Vermeulen, E. Ros, K.I. Kellermann, M.H. Cohen, J.A. Zensus & H.J. van Langevelde, H. J., Astronomy and Astrophysics, v.401, p.113-127 (2003).
[18] R. C. Walker, J. D. Romney & J. M. Benson, The Astrophysical Journal, Part 2 - Letters, vol. 430, no. 1, p. L45-L48.
[19] M. L. Lister, M. H. Aller, H. Aller, T. Hovatta, T.; K. I. Kellermann…., The Astrophysical Journal, Volume 742, Issue 1, article id. 27 (2011).
[20] D. C. Homan, M. Kadler, K. I. Kellermann, Y. Y. Kovalev, M. L. Lister, E. Ros, T. Savolainen, & J. A. Zensus, *Astrophysical Journal*, 706: 1253-1268 (2009).
[21] J. D. Jackson, "Classical Electrodynamics", Wiley 3rd Ed.
[22] C. Flynn, *"Synchrotron radiation notes"*, http://www.astro.utu.fi/~cflynn/astroII/l4.html.
[23] E. Ros 2008, "Kinematics of AGN jets", J. Phys.: Conf. Ser. 131 012061.
[24] S. C. Unwin *et al.* 2001, "Superluminal Motion", Encyclopedia of Astronomy and Astrophysics, edited by Paul Murdin, article 2357. Bristol: Institute of Physics Publishing.
[25] R. D. Blandford *et al.* 1987, "Superluminal Radio Sources" , ed. J. A. Zensus & T. J.Pearson (Cambridge: Cambridge University Press), p. 129.
[26] R. C. Vermeulen, E. Ros, K. I. Kellermann, M. H. Cohen, J. A. Zensus & H. J. van Langevelde, 2003, A&A, 401, 113.
[27] Kadler, M., Ros, E., Lobanov, A. P., Falcke, H., & Zensus, J. A. 2004, A&A, 426, 481.
[28] E. Ros & M. Kadler, "Powering the jets in NGC 1052" (2008), J. Phys.: Conf. Ser. 131 012056.
[29] P. J. Napier, D. S. Bagri, B. G. Clark, A. E. E. Rogers, J. D. Romney, A. R. Thompson, R. C. Walker, Proc. IEEE, Vol. 82, No. 5, p. 658 – 672.
[30] E. Ros (2011), "High-resolution monitoring of parsec-scale jets in the Fermi era", Fermi & Jansky Proceedings - eConf C1111101.
[31] J.F. Hemboldt et al., "The VLBA Imaging and Polarimetry Survey at 5 GHz", ApJ 658, 203, 2007.
[32] J.D. Linford et al., "Characteristics of Gamma-Ray Loud Blazars in the VLBA Imaging and Polarimetry Survey", ApJ 726, 16, 2011.
[33] A. Marscher *et al.*, "Multi-Waveband Emission Maps of Blazars", Jou. of Astron. & Astrop. 32, 233, 2011.
[34] J.A. Zensus et al., "Sub-milliarcsecond Imaging of Quasars and Active Galactic Nuclei. II. Additional Sources", AJ 124, 662, 2002.

[35] TANAMI - Tracking Active Galactic Nuclei with Austral Miliarcsecond Interferometry http://pulsar.sternwarte.uni-erlangen.de/tanami/.
[36] R. Ohja, M. Kadler, M. Böck, R. Booth, M. S. Dutka, P. G. Edwards, …, Astronomy and Astrophysics, Volume 519, id.A45.
[37] M. H. Cohen, M. L. Lister, D. C. Homan, M. Kadler, K. I. Kellermann, Y. Y. Kovalev & R. C. Vermeulen, 2007, ApJ, 658, 232.
[38] S. Britzen *et al*. 2008, "A multi-epoch VLBI survey of the kinematics of CFJ sources", A&A, 484, 119.
[39] D. C. Homan, R. Ojha, J. F. C. Wardle, D. H. Roberts, M. F. Aller, H. D. Aller & P. A. Hughes, 2001, ApJ, 549, 840.
[40] B. G. Piner, D. Bhattarai, P. G. Edwards & D. L. Jones, 2006, ApJ, 640, 196.
[41] K. I. Kellermann 2004, ApJ, 609, 539.
[42] J. A. Zensus *et al*., Annu. Rev. Astron. Astrophys. 1997. 35:607–36.
[43] K.I. Kellermann, Y.Y. Kovalev, M.L. Lister, D.C. Homan, M. Kadler, M.H. Cohen, E. Ros, J.A. Zensus, R.C. Vermeulen, M.F. Aller, H.D. Aller, Astrophysics and Space Science, 311, Issue 1-3, 231-239 (2007).
[44] M. Camenzind & M. Krockenberger 1992, Astron. Astrophys. 255, 59–62.
[45] P. E. Hardee *et al.* 1987, Ap. J. 318, 78–92.
[46] A. Königl & A. R. Choudhuri 1985, Ap. J. 289, 173–87.
[47] M. Camenzind *et al.* 1986, Astron. Astrophys 156, 137–51.
[48] S. J. Qian, T. P. Krichbaum, A. Witzel, A. Quirrenbach, C. A. Hummel & J. A. Zensus 1991, *Acta Astro. Sinica* 32(4):369–79. *Transl. Chin. Astron. Astrophys.* 16:137–47.
[49] S. J. Qian, T. P. Krichbaum, J. A. Zensus, W. Steffen & A. Witzel 1996, *Astron. Astrophys.* 308, 395– 402.
[50] A. Alberdi (1997), "The high-frequency compact radio structure of the peculiar quasar 4C 39.25", Astronomy and Astrophysics, v.327, p.513-521.
[51] D. C. Homan *et al*. 2008, "Physical properties of jets in AGN", International Journal of Modern Physics: Conference Series Vol. 8 (2012) 163–171.
[52] Y. Y. Kovalev *et al*., Astrophys. J. 696, L17 (2009).
[53] J. M. Paredes, V. Bosch-Ramon & G. E. Romero 2006, A&A 451, 259.
[54] http://www.nrao.edu/pr/2000/vla20/background/superlum/.